

The Propagation of Compressional Alfvén Waves in Nonuniform Plasmas

R. Morrow^{A,B} and M. H. Brennan^A

^A School of Physical Sciences, Flinders University of South Australia, Bedford Park, S.A. 5042.

^B Present address: Electricity Council Research Centre, Capenhurst, Cheshire, England.

Abstract

A theoretical treatment is presented for the propagation of Alfvén waves in a plasma. It includes the effects of resistivity, ion-neutral collisions, the ion cyclotron frequency and radial nonuniformities in ion density, neutral particle density and temperature. The theory is applied to plasmas with conducting and nonconducting walls and the results are compared with those of experiments conducted in the afterglow of a shock-produced plasma. Nonuniformity in the ion density is found to have a marked effect on the dispersion relation and wave field profiles, while nonuniformities in the total particle density and temperature are less important. Excellent agreement is obtained between theory and experiment and this allows unambiguous and accurate determinations to be made of the average total particle density, which is found to be ~50% of the initial filling density, and of the cross section for momentum transfer between protons and hydrogen atoms.

1. Introduction

The hydromagnetic oscillations of a radially uniform cylindrical plasma have been investigated by a number of authors. The most general theoretical solution of this problem has been presented by Woods (1962) who retained all the dissipative and other second-order effects for a radially uniform plasma. Generally good agreement has been found between theory and experiment for both the compressional (or fast) and the torsional (or slow) Alfvén waves over a wide range of frequencies.

Confining our attention to the compressional wave, which is the subject of the present work, we note particularly the experimental work of Swanson *et al.* (1964), Malein (1965) and Cross and Lehane (1967). In each experiment, one or more parameters in the theory were adjusted to bring the predicted dispersion relation into agreement with experiment. Thus Swanson determined the degree of ionization, the resistivity and the ion-neutral collision frequency in his experiment. Malein, using a theoretical value for the momentum transfer cross section, determined the neutral particle density from such a fitting procedure. In these experiments, and in the theory of Woods, the plasma was assumed to be radially uniform.

The effects of density gradients on the propagation of compressional Alfvén waves in a resistiveless plasma have been considered theoretically by Pneuman (1965), Cross and Lehane (1968) and Morrow and Brennan (1971). Pneuman's theory was limited to frequencies less than the ion cyclotron frequency ω_{ci} , and required a moving plasma-vacuum boundary. Cross and Lehane modified this theory so that it applied to a plasma with conducting walls and found a special case of the solution at $\omega = \omega_{ci}$. They and Pneuman only considered density profiles in the form $n = n_0 (1 - r^2/a^2)$,

where n_0 is the peak density, r the radial distance and a the plasma radius. Morrow and Brennan (1971) numerically solved the relevant differential equation to find solutions which were valid from low frequencies through the ion cyclotron region to frequencies less than one-tenth the electron cyclotron frequency and which were applicable to a plasma with an arbitrary density distribution. Both Cross and Lehane, and Morrow and Brennan found fair agreement between the calculated and measured wave field profiles. For high frequencies, where the compressional wave becomes the helicon wave, Blevin and Christiansen (1968) found good agreement between their experimental results and a theory which included resistivity and the electron cyclotron resonance (Davies and Christiansen 1969).

The present work extends both the theoretical and experimental investigations of the compressional wave, with special emphasis on the effects of radial nonuniformities on the dispersion relation and the field profiles. The comprehensive nature of the theoretical treatment facilitates calculations for both conducting and nonconducting boundaries. A more accurate treatment of the ion-neutral momentum transfer cross section, developed by Brennan and Morrow (1971), also enables an unambiguous determination of this cross section to be obtained from measurements of the dispersion of compressional waves in a laboratory plasma.

2. Theory

We restrict our discussion to small amplitude low-frequency waves ($\omega \lesssim 0.1 \omega_{ce}$), with axisymmetry ($m = 0$), propagating in a hydrogen plasma. The basic equations (the equation of motion, the generalized Ohm's law and Maxwell's equations) readily yield an equation for the wave magnetic field \mathbf{b} ,

$$\begin{aligned} \mathbf{b} + \nabla \times [(B_0^2/\omega^2 \rho' \mu_0) \{(\nabla \times \mathbf{b}) \times \hat{\mathbf{z}}\} \times \hat{\mathbf{z}} \\ + (iB_0/\omega en\mu_0)(\nabla \times \mathbf{b}) \times \hat{\mathbf{z}} + (\omega\mu_0)^{-1} \boldsymbol{\eta} \cdot \nabla \times \mathbf{b}] = 0, \end{aligned} \quad (1)$$

where we have assumed that the wave propagation is in the direction of the unit vector $\hat{\mathbf{z}}$. The steady axial magnetic field is $\mathbf{B} = B_0 \hat{\mathbf{z}}$; the equilibrium macroscopic ion velocity, current density, and electric field are zero; the plasma resistivity is represented by the resistivity tensor $\boldsymbol{\eta}$; n is the ion number density and ρ' is a complex mass density given by the expression

$$\rho' = \rho_i + \rho_n/(1 - i\omega\tau),$$

where ρ_i and ρ_n are the ion and neutral particle mass densities, and

$$\tau^{-1} = (\frac{2}{3}\sqrt{2}) n Q_D \bar{v}.$$

We have also assumed that the ions and neutrals are in equilibrium at the same temperature T , with an average particle velocity \bar{v} . The factor Q_D is the ion-neutral momentum transfer cross section for an incident ion energy of $5kT$ (Brennan and Morrow 1971).

Equation (1) is the same basic equation as that obtained by De Silva (1961) and others for a uniform plasma. However, we here retain the possibility of radial variations in the ion density, the neutral density and the temperature.

(a) Uniform Plasma with Conducting Boundary

Before proceeding to the solution of equation (1) for the general case, it is useful to consider the solution for a uniform plasma bounded by a conducting wall at $r = a$. If we define the operator S as

$$S = \partial^2/\partial r^2 + r^{-1} \partial/\partial r - r^{-2}$$

then equation (1) may be written in cylindrical component form as

$$(S + \gamma_1^2)(S + \gamma_2^2) \{b_r \hat{r} + b_\theta \hat{\theta} - (\partial b_z/\partial r) \hat{z}\} = 0, \quad (2)$$

where γ_1 and γ_2 are functions of the plasma parameters and the wave frequency (see e.g. De Silva 1961). The operator $S + \gamma_1^2$ is Bessel's operator for the first-order Bessel function. The requirement that the wave fields are finite at the origin thus leads to the solution for the b_r component, for example,

$$b_r = A_1 J_1(\gamma_1 r) + A_2 J_1(\gamma_2 r).$$

In general, both γ_1 and γ_2 are complex, and the boundary conditions in a given problem will require the use of both. However, with the exception of Swanson *et al.* (1964), previous workers have neglected one of the γ_i and assumed that the γ used was real and defined by the relation $J_1(\gamma a) = 0$. This approach leads to a dispersion relation in the form of a quadratic in k^2 . Swanson *et al.* calculated the real and imaginary parts of γ_1 for typical plasma conditions and found that the imaginary part was indeed very small ($\lesssim 0.3\%$) compared with the real part and that deviations of the real part from the value given by $J_1(\gamma a) = 0$ were also small ($\lesssim 0.3\%$). They did not quote values for γ_2 .

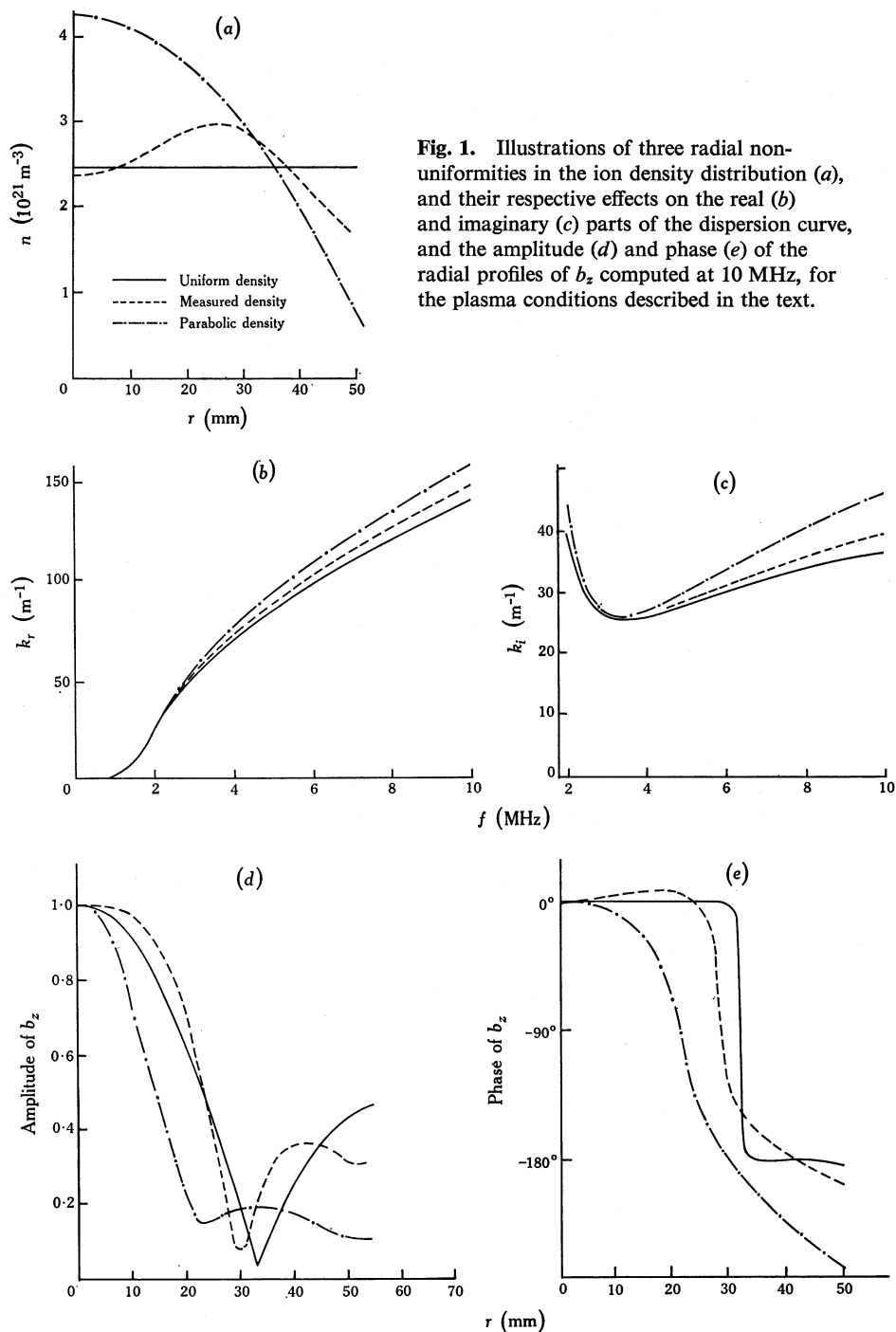
It is instructive to obtain the solution to the dispersion relation, retaining both of the γ_i , to see why γ_2 can be ignored for the uniform plasma. We have obtained the solution to such a dispersion relation by numerical methods, using the r and θ components of equation (2) together with the two boundary conditions used by Davies and Christiansen (1969) in their treatment of the high frequency branch of the dispersion relation (helicon waves):

$$(b_r)_{r=a} = 0 \quad \text{and} \quad (\partial b_\theta/\partial r + r^{-1} b_\theta)_{r=a} = 0.$$

We find, as did Swanson *et al.* (1964), that the values of k computed from the 'two γ ' dispersion relation are within 1% of those obtained from the 'one γ ' dispersion relation of De Silva (1961) and others, over a wide range of frequencies. For example, for waves propagating at 6 MHz in hydrogen with $B_0 = 0.8$ T, $n = 2 \times 10^{21} \text{ m}^{-3}$, $T = 10^4$ K and a neutral particle density of $8 \times 10^{21} \text{ m}^{-3}$, the values of γ_i (in complex notation) are given by

$$\gamma_1 a = (3.81, 0.007) \quad \text{and} \quad \gamma_2 a = (6.88, 15.74).$$

The value of γa computed from $J_1(\gamma a) = 0$ is $\gamma a = (3.83, 0)$. We see that $\gamma_1 \approx \gamma$ and γ_2 has a large imaginary part. Thus $J_1(\gamma_2 r)$ behaves very much like I_1 , a modified Bessel function of the first kind which diverges as r increases. Furthermore, since terms in γ_2 enter the expressions for b_r and b_θ in the form $J_1(\gamma_2 r)/J_1(\gamma_2 a)$, they have



little effect except near the boundary. We note, in passing, that it is precisely this feature that makes it possible to match the boundary conditions for nonconducting walls, where the conducting wall condition $(b_r)_{r=a} = 0$ is replaced by the requirement that b_r , which is in general nonzero at a nonconducting boundary, is continuous across the boundary.

(b) Nonuniform Plasma with Conducting Boundary

In order to obtain the dispersion relation and radial wave field profiles for compressional Alfvén waves in a plasma including effects due to resistivity, neutral particles, and nonuniformities in the ion density, neutral density and temperature, the appropriate components of equation (1) must be integrated numerically. For computational convenience, we choose to work with the r and θ components of equation (1). The equations are solved, subject to the boundary conditions, as four simultaneous complex first-order differential equations by using the fourth-order Runge-Kutta integration method. The starting values for the integration, which begins at the origin, are obtained from the uniform plasma solution discussed in subsection (a) above.

The input data to the calculation, which was performed on the Adelaide University CDC 6400 computer, specify the plasma conditions, including any measured or assumed radial variations in densities or temperature, and the wave frequency. The output gives the real and imaginary parts of the wave number and the radial dependence of the amplitudes and phases of the wave magnetic fields.

Since it is difficult to determine experimentally the radial variations in all three plasma parameters (ion density, neutral density, temperature), computations were first performed to evaluate the effects of radial variations in each of these parameters on the wave dispersion and field profiles. The gas used was hydrogen, and a standard set of average plasma conditions (corresponding quite closely to actual experimental conditions) was used in each computation:

tube radius	$a = 50 \text{ mm},$
magnetic field	$B_0 = 0.8 \text{ T},$
momentum transfer cross section	$Q_D = 8.0 \times 10^{-19} \text{ m}^2,$
average ion density	$n = 2.45 \times 10^{21} \text{ m}^{-3},$
average total density	$n_T = 10 \times 10^{21} \text{ m}^{-3},$
average temperature	$T = 1.06 \times 10^4 \text{ K}.$

Fig. 1a shows the three ion density distributions chosen to determine the effects of radial variations in ion density, keeping total density and temperature uniform. All three ion density distributions are normalized to the same average density. Figs 1b and 1c show the effect of these distributions on the real and imaginary parts of the wave number. We note that, as the frequency decreases, the curves for both k_r and k_i merge at $f \approx 3 \text{ MHz}$ whereas for the resistiveless case the curves for k_r remain separated (Morrow and Brennan 1971). This effect is primarily due to the increased coupling between ions and neutrals at lower frequencies, which results in an effectively uniform mass density across the tube despite significant radial variations in ion density.

The amplitudes and phases of the axial magnetic field component b_z are shown in Figs 1*d* and 1*e* for 10 MHz, the highest frequency considered. We note the marked departures of these curves from the $J_0(\gamma r)$ Bessel function distribution, which holds for the uniform resistiveless plasma. Calculations of the Poynting vector show that there is a flow of energy from regions of lower density towards regions of higher density. Thus, with resistivity and ion-neutral collisions, the wave in a nonuniform plasma is refracted towards the high density regions, and this produces a phase velocity that is less than that for a uniform plasma of the same average density. Although the curves for b_θ and b_r are not given, they show similar departures from the Bessel function shape (in this case, $J_1(\gamma r)$). In particular, b_θ is not zero at the boundary but is always small ($\lesssim 10\%$ of the maximum value for the uniform plasma) and approaches zero as the plasma density at the boundary approaches zero.

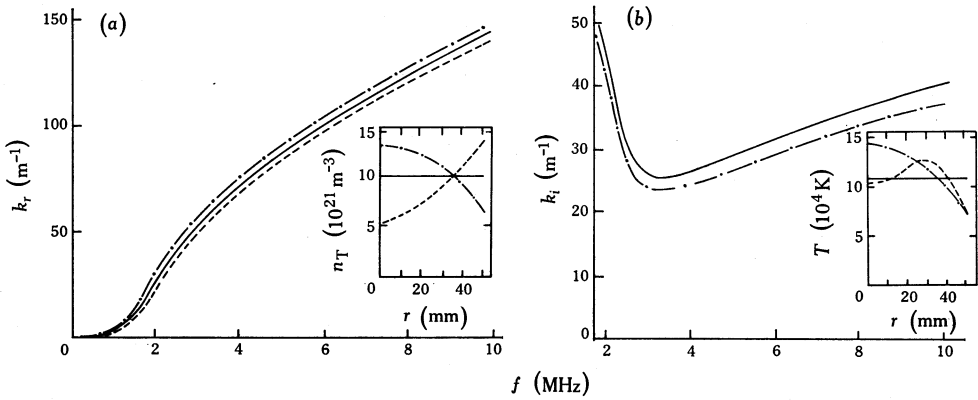


Fig. 2. (a) Real part of the dispersion curve computed for the three total particle distributions shown in the inset and under the plasma conditions described in the text. (b) Imaginary part of the dispersion curve computed for the three temperature distributions shown in the inset and under the plasma conditions described in the text. The results for the parabolic and 'annular' temperature distributions are so close that they are both represented by the dot-dash dispersion curve.

The effect on the dispersion relation of varying the total particle density distribution is considerably less than the effect of similar variations in ion density. As an example, Fig. 2*a* shows the effect on the real part k_r of the wave number of the very large differences in total particle distributions shown in the inset. Each curve is obtained for the same ion density distribution, which was chosen to be the measured ion density of Fig. 1*a*. We note that, despite the very marked differences in the total particle distributions, the effect on k_r is less than that shown in Fig. 1*b* except at low frequencies. It is also of interest to note that the effect on k_r is not very frequency dependent. The effect of radial variations in total particle density on the imaginary part of the wave number is similar, being relatively small and not strongly frequency dependent.

The effect on the dispersion relation of radial variations in temperature is also small. Again, we choose conditions similar to those encountered in the experiments: the measured ion density of Fig. 1*a* and a uniform total particle distribution. We find that radial variations in temperature have a relatively minor effect on k_r . The effect on k_i is somewhat larger although still considerably less than the effects produced by radial variations in ion density. As an example, Fig. 2*b* shows the effect on k_i of the

three temperature profiles shown in the inset. Clearly, radial variations in temperature have only a small effect on the dispersion curves. In later comparisons between theory and experiment, we make only a small error by assuming that the radial temperature profile has the same shape as the ion density profile.

It is of interest to note that a nonuniform temperature distribution results in reduced damping. This effect was predicted by Woods (1963). Our calculations of the Poynting vector show that this effect results from the refraction of the wave towards regions of higher temperature and hence of smaller resistivity.

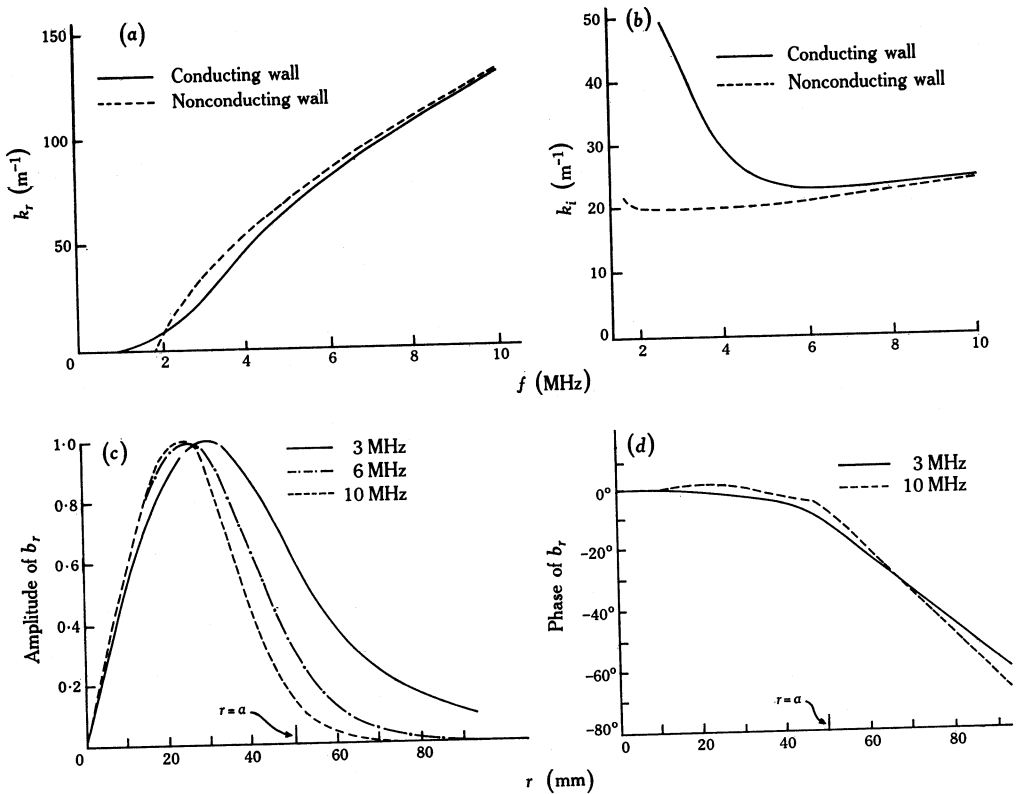


Fig. 3. Comparison of the real (a) and imaginary (b) parts of the dispersion curves obtained with conducting and nonconducting boundaries for the plasma conditions described in the text. Amplitude (c) and phase (d) of b_r as computed with the nonconducting wall theory are shown for the plasma conditions described in the text. Note that the 6 MHz phase curve is not shown because it lies too close to the other curves. The plasma radius is 50 mm.

(c) Nonuniform Plasma with Nonconducting Boundary

The method of solution of equation (1) for a plasma with a nonconducting boundary at $r = a$ closely parallels that used for the conducting boundary case. Again, we consider the r and θ components of the equation, integrating out from the origin. At the boundary, the fields in the plasma must be matched to the vacuum fields. Since the wave frequencies are low we may neglect the displacement current and obtain for the vacuum wave magnetic field

$$\mathbf{b} = A_1 K_1(kr) \hat{\mathbf{r}} - i A_1 K_0(kr) \hat{\mathbf{z}},$$

where K_0 and K_1 are modified Bessel functions of the second kind of orders zero and one. We now require three boundary conditions at $r = a$ rather than two as in the conducting boundary case. These are readily obtained from Maxwell's equations and the requirement that surface currents of infinite density cannot occur in a plasma with finite resistivity:

$$\begin{aligned} [b_r]_{r=a} &= 0, & \text{'jump' in } b_r &= 0; \\ (b_\theta)_{r=a} &= 0, & b_\theta &\text{ zero at boundary;} \\ [\partial b_r / \partial r]_{r=a} &= 0, & \text{'jump' in } \partial b_r / \partial r &= 0. \end{aligned}$$

The results of a typical calculation for a plasma with nonconducting walls are shown in Fig. 3. In Figs 3*a* and 3*b* we compare the real and imaginary parts of the dispersion relation for identical plasmas with conducting and nonconducting walls. The plasma conditions used for the calculations are a magnetic field of 0.8 T, the measured ion density of Fig. 1*a*, a temperature profile with the same shape as the ion density profile and an average value of 1.02×10^4 K, a uniform total particle density of $5.4 \times 10^{21} \text{ m}^{-3}$ and an ion-neutral collision cross section of $5.1 \times 10^{-19} \text{ m}^2$.

The radial dependences of the amplitude and phase of the b_r field component are shown in Figs 3*c* and 3*d* for three wave frequencies. We note that, whereas at high frequencies the wave fields are largely confined to the plasma, at low frequencies the fields penetrate for a considerable distance into the vacuum region. This behaviour results in the very significant difference that occurs at low frequencies between the dispersion curves for conducting and nonconducting walls. In particular we note that, even though there is a relatively sharp cut-off frequency for the nonconducting wall case, the damping remains relatively small because an increasing proportion of the wave energy is stored in the vacuum as the frequency decreases, leaving less energy in the plasma to be dissipated.

3. Experimental Apparatus

The experiments were carried out using the plasma source FPS-1, described by Blackburn *et al.* (1969). The cylindrical glass vacuum vessel is 0.9 m long and 102 mm in diameter. When conducting wall boundary conditions are required, a 100 mm diameter stainless steel tube can be inserted into the vacuum vessel. A residual gas pressure of 3×10^{-6} torr is achieved by conventional pumping methods. For the wave experiments, hydrogen is continuously admitted to the vacuum vessel through a palladium leak. The resulting working gas pressure is 0.15 torr.

The vacuum vessel is enclosed by solenoid coils energized by a capacitor bank, enabling axial magnetic fields of up to 0.8 T to be achieved. The rise time of the field is approximately 10 ms and the plasma is produced at the time of peak magnetic field. The plasma is produced by a normal ionizing shock wave which is driven down the tube by a square current pulse of amplitude ~ 45 kA and duration $\sim 40 \mu\text{s}$. The current in the plasma is produced by discharging a fast capacitor bank through a pair of coaxial electrodes located at one end (the 'firing' end) of the vacuum vessel. A schematic diagram of the source is shown in Fig. 4.

Electron density measurements were made using an eight-channel polychromator (Stirling and Westwood 1968) to observe the Stark broadening of the H_β line of

hydrogen. Radial density profiles were obtained by observing along optic axis 1 (OA1) of Fig. 4, located at different radial positions. The average density in the wave propagation region could be monitored by making observations along optic axis 2 (OA2).

The compressional waves were launched 100 μs after the plasma preparation pulse had ended, by means of a 40 mm diameter copper launching loop (WLL) shown in Fig. 4. The loop, which was encased in glass, was positioned ~ 100 mm from the receiving end plate and was concentric with the tube axis. A damped oscillating current was produced in the launching loop by discharging a variable number of capacitors into the inductive circuit of the single turn loop and the coaxial lead. The arrangement provided axial wave magnetic fields of 20–30 mT at frequencies up to 10 MHz. The waves were detected with 40-turn centre-tapped coils sealed into the tips of 6 mm quartz tubes. As shown in Fig. 4, the probes could be inserted into the vacuum vessel at three points to enable determination of the spatial dependence of the three components of the wave magnetic fields.

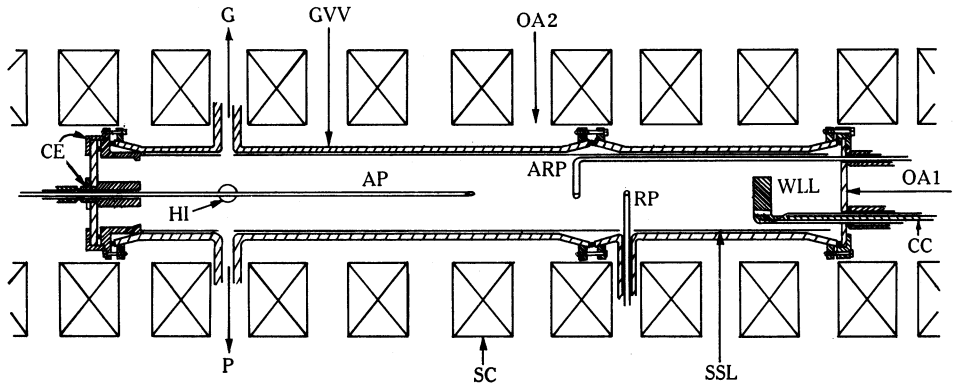


Fig. 4. Plasma source FPS-1. The abbreviations used are: G, gauges; GVV, glass vacuum vessel; OA2, optic axis 2; CE, concentric electrodes; HI, hydrogen inlet; AP, axial probe; ARP, axial and radial probe; RP, radial probe; WLL, wave launching loop; OA1, optic axis 1; CC, coaxial conductor; P, pumps; SC, solenoid coils; SSL, stainless steel liner.

4. Results and Discussion

(a) Conducting Boundary

The dispersion relation and the radial wave field profiles with a conducting boundary were determined experimentally for two values of the steady axial magnetic field. Only the results for 0.8 T are presented here. The results for 0.4 T, experimental checks on the existence of only the lowest order radial wave mode, and results for a deuterium plasma have been given by Morrow (1970). We also restrict our discussion to the radial profile of the b_z component of the wave field; the profiles for b_θ and b_r have been presented by Morrow.

Radial profiles of the b_z component of the wave, wave velocity and attenuation were obtained for six frequencies in the range 3–10 MHz for a hydrogen plasma with the measured radial density distribution shown in Fig. 5a. For these experiments the wave launcher was positioned 100 mm from the receiving end plate and the waves were detected by the axial and radial probe (ARP) shown in Fig. 4.

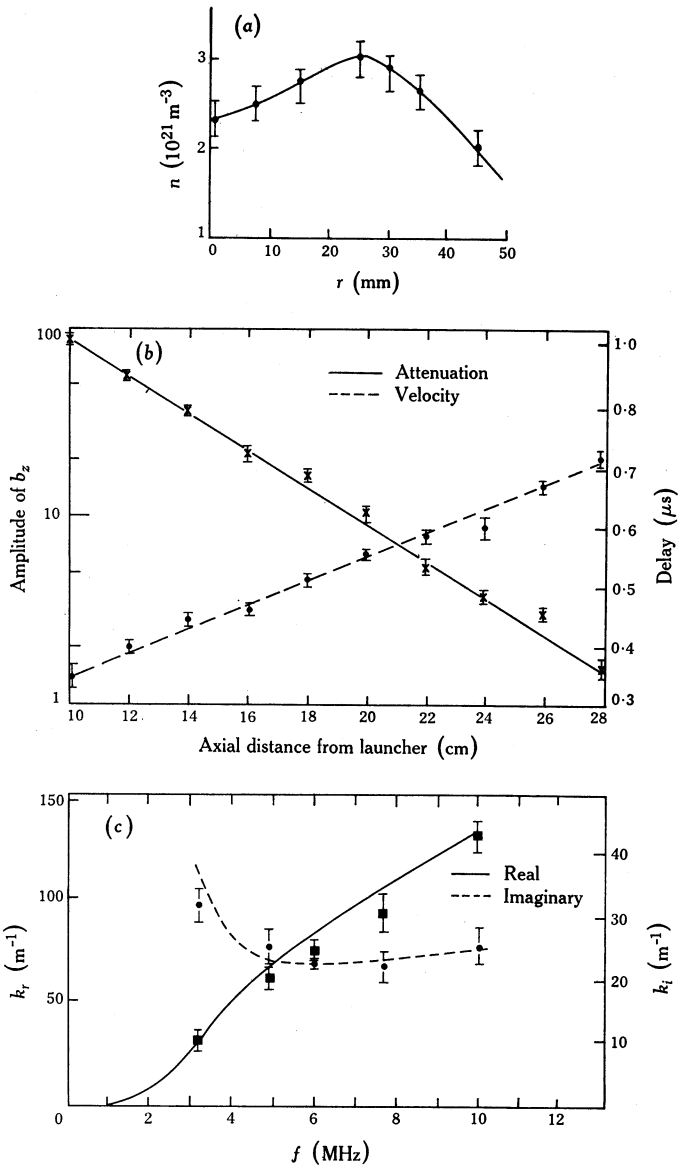


Fig. 5. (a) Radial density profile (full circles) determined from Stark broadening measurements for hydrogen at 150 mtorr and 0.8 T. The solid line is the polynomial fit used in the calculations. Attenuation and velocity measurements (b) for the compressional wave at 6 MHz and dispersion curves (c) for compressional waves are shown for the above-mentioned plasma conditions.

Wave velocity and attenuation were obtained by measuring the time of arrival and amplitude of the b_z wave signal at the centre of the tube for different axial positions. A typical set of results is shown in Fig. 5b. From these measurements the real and imaginary parts of the wave number could be determined, the values so obtained being shown in Fig. 5c together with the theoretical curves obtained by a least squares fitting

method (Morrow 1970). In this method, we assume that the radial electron temperature distribution has the same shape as the ion density distribution with a mean value of 1.02×10^4 K, equal to that obtained from spectroscopic observations. The total particle density n_T is assumed to be uniform across the radius of the tube, and this quantity, together with Q_D , is then used as a variable parameter in the fitting procedure.

The sensitivity of the fit to variations in Q_D and n_T is shown in Figs 6*a* and 6*b*. Clearly, the fit is more sensitive to a change in the total particle density than to a change in the cross section. If we take as a measure of the error in each of these quantities the values at 1.5 times the best-fit r.m.s. percentage error, we obtain

$$n_T = (5.4 \pm 0.8) \times 10^{21} \text{ m}^{-3} \quad \text{and} \quad Q_D = (6.0^{+3.0}_{-2.0}) \times 10^{-19} \text{ m}^2.$$

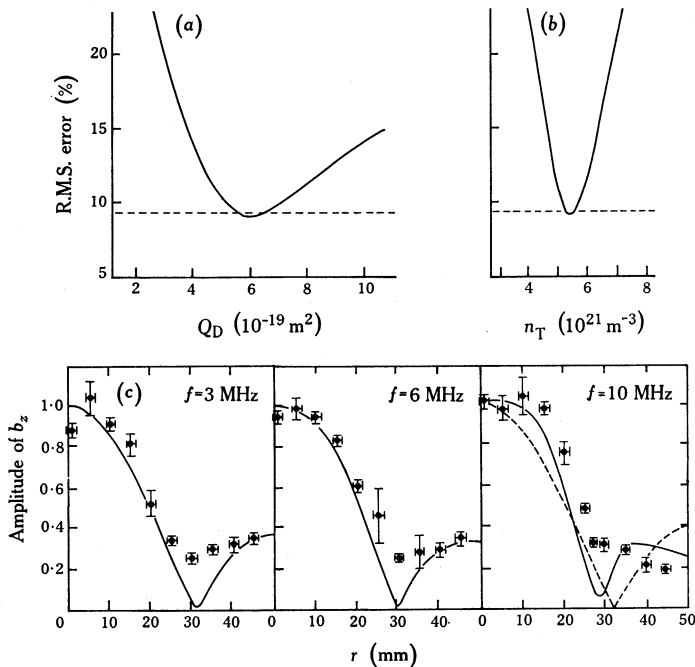


Fig. 6. Sensitivity of the r.m.s. error between theory and experiment to variations in (a) cross section for $n_T = 5.4 \times 10^{21} \text{ m}^{-3}$ and (b) total particle density for $Q_D = 6.0 \times 10^{-19} \text{ m}^2$. The dashed lines indicate the r.m.s. percentage errors of the experimental results. Part (c) shows a comparison between measured b_z profiles (full circles) and theoretical profiles (solid curves), computed using the best fit values of Q_D and n_T shown in (a) and (b), for hydrogen at 150 mtorr and 0.8 T. The dashed curve is the theoretical profile for a uniform plasma.

The value for Q_D , which has already been reported by Brennan and Morrow (1971), is in good agreement with theoretical calculations and with measurements of the scattering cross section. The value for n_T is $\sim 50\%$ of the initial filling density ($1.1 \times 10^{22} \text{ atoms m}^{-3}$). This result for the afterglow of a shock-produced plasma is similar to the results obtained by other workers, notably Forman (1966) and Cross and Lehane (1967, 1968). It is of interest to compare the above results with the best fit values for Q_D and n_T that are obtained if the plasma is assumed to be completely uniform with

the same average ion density and temperature:

$$n_T = 5.0 \times 10^{21} \text{ m}^{-3} \quad \text{and} \quad Q_D = 9.1 \times 10^{-19} \text{ m}^2.$$

Thus the plasma nonuniformity has only a small effect on the value deduced for the total particle density, but a very large effect on that for the momentum transfer cross section.

The results of measurements of the radial variation of b_z are shown in Fig. 6c for 3, 6 and 10 MHz. Also shown are the theoretical profiles computed using the best fit values of Q_D and n_T shown in Figs 6a and 6b and the measured ion density profile of Fig. 5a. The computed profile for a uniform plasma is also shown for the 10 MHz case. It is of interest to note the relatively small difference between these theoretical profiles and those for the resistiveless case reported by Morrow and Brennan (1971). It is also of interest to note that the experimental results do not exhibit the deep minimum of the theory. This effect, which has been observed by other workers, is presumably due to the finite size of the probe and its influence on the wave currents, particularly in the vicinity of the field minimum which corresponds to a maximum in the wave currents.

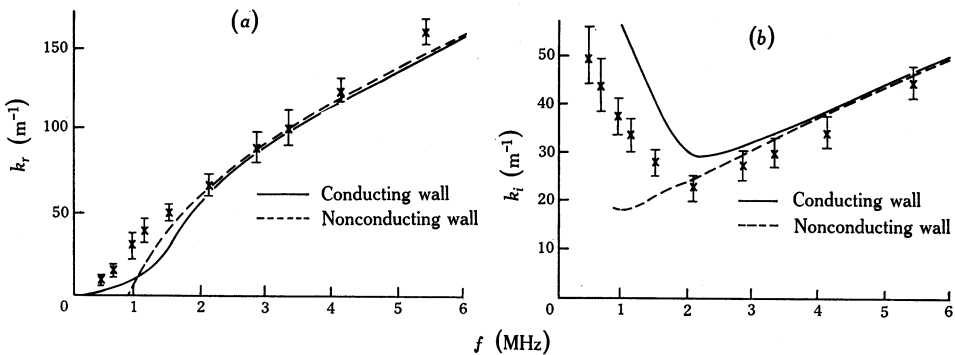


Fig. 7. Comparison of experimental results (crosses) for the (a) real and (b) imaginary parts of the dispersion curves for nonconducting walls with the indicated theoretical results (curves) computed for $n_T = 5.4 \times 10^{21} \text{ m}^{-3}$ and $Q_D = 6.0 \times 10^{-19} \text{ m}^2$.

(b) Nonconducting Boundary

Prior to performing the experiments with a conducting boundary, we carried out some experiments with a nonconducting boundary. The measurements, although somewhat preliminary, are presented here. The only other experimental work on compressional Alfvén waves with a nonconducting boundary appears to be that of Jephcott and Malein (1964) and Malein (1965), in which a conducting wall was placed in contact with the outside surface of the glass vacuum vessel. The present experiments were performed in hydrogen at a pressure of 0.15 torr and a magnetic field of 0.4 T. The wave launcher was that used for the conducting wall case and the waves were detected by the axial probe (AP) shown in Fig. 4. Thus only the on-axis amplitude and arrival time of the b_z component of the wave were determined.

The determination of ion density was limited to observations of Stark broadening using optic axis 2 (OA2) of Fig. 4, i.e. across the tube. The 'average' density so

obtained was $3.0 \times 10^{21} \text{ m}^{-3}$ at the time of wave launching. For the purpose of calculating theoretical dispersion curves it was assumed that the density profile had the same shape as that shown in Fig. 5a, but with an average value of $3.0 \times 10^{21} \text{ m}^{-3}$. The temperature and total particle density were assumed to be the same as those determined for the conducting boundary case at 0.8 T. With these rather approximate plasma parameters we cannot expect a good fit to the experimental results. However, the theory should provide a semiquantitative description of the results.

The experimental results are shown in Fig. 7 together with the computed dispersion curves for conducting and nonconducting walls. Above 2.8 MHz there is little difference between the computed dispersion curves for conducting and nonconducting walls, and the fit between theory and experiment is surprisingly good. Below 2.8 MHz the experimental values diverge quite markedly from both theoretical curves in a way which suggests that the waves are behaving as though they are propagating in a plasma with conducting walls and with a lower cut-off frequency than used in the theory.

The agreement between theory and experiment at high frequencies indicates that the approximate plasma parameters used in the theory adequately describe the plasma. The behaviour at low frequencies is presumably due to the interaction of the vacuum fields of the wave (which are quite large and extensive at low frequencies) with the solenoid coils used to produce the axial magnetic field. These coils, which are ~ 7 cm long with gaps of ~ 5 cm, will act like a continuous conductor at low frequencies. The wave will thus exhibit a cut-off frequency which, because of the larger diameter, will be at a lower frequency than for the case when the conductor is at the vacuum vessel wall.

5. Conclusions

Our results show that radial nonuniformities in plasma parameters have significant effects on the propagation characteristics of compressional Alfvén waves. Nonuniformities in the ion density have the largest effect and must be taken into account before good agreement can be achieved between theory and experiment. Radial nonuniformities in temperature and total particle density have less effect, although it is useful to take some account of the effect of radial nonuniformities in temperature on the attenuation length.

The excellent fit between theory and experiment has enabled us to determine values for the total particle density in the afterglow of a shock-produced plasma and the cross section for momentum transfer between protons and hydrogen atoms. The values obtained are free from the uncertainties of earlier determinations in which a uniform ion density was assumed. In particular, we have shown that the assumption of uniform density for a plasma with a known nonuniform density produces an overestimate of the momentum transfer cross section. For the chosen plasma conditions, which are typical of those used by earlier workers such as Cross and Lehane (1967, 1968), the error made is as much as 50%. The average total particle density is, on the other hand, well determined even if a uniform ion density is assumed.

The completeness of our treatment of the effects of plasma nonuniformities, ion-neutral collisions and resistivity enables us to evaluate also the range of validity of previous approximate theories. In particular, the quadratic solution developed by De Silva (1961), Woods (1962) and others accurately predicts the phase velocity at low frequencies. Nonuniformities in ion and neutral particle density have only minor

effects on the wave attenuation. However, a nonuniform temperature distribution will lower the wave attenuation below that for a uniform temperature distribution at all frequencies.

The solution presented for the compressional wave propagating in a plasma with a nonconducting boundary is the first to include ion-neutral collisions, the $v \times B$ term, the ion cyclotron term and the effect of large resistivity, as well as to extend the theory to include the effects of plasma nonuniformities. The theory agrees well with the experimental results at high frequencies. Better agreement at low frequencies could presumably be achieved by including effects due to conductors, such as solenoid coils, that are external to the plasma.

Acknowledgments

The authors acknowledge the financial support provided for this work by the Australian Institute of Nuclear Science and Engineering and the Australian Research Grants Committee. They also acknowledge helpful discussions with Dr H. A. Blevin, Dr B. Davies and Dr P. F. Liddle.

References

- Blackburn, T. R., Brennan, M. H., and Fletcher, J. (1969). *Plasma Phys.* **11**, 655.
 Blevin, H. A., and Christiansen, P. J. (1968). *Plasma Phys.* **10**, 799.
 Brennan, M. H., and Morrow, R. (1971). *J. Phys.* B **4**, L53.
 Cross, R. C., and Lehane, J. A. (1967). *Nucl. Fusion* **7**, 219.
 Cross, R. C., and Lehane, J. A. (1968). *Physics Fluids* **11**, 2621.
 Davies, B., and Christiansen, P. J. (1969). *Plasma Phys.* **11**, 987.
 De Silva, A. W. (1961). Lawrence Radiation Lab. Rep. No. UCRL-9601 (Ph.D. Thesis).
 Forman, P. R. (1966). Lawrence Radiation Lab. Rep. No. UCRL-17177 (Ph.D. Thesis).
 Jephcott, D. F., and Malein, A. (1964). *Proc. R. Soc. A* **278**, 243.
 Malein, A. (1965). *Nucl. Fusion* **5**, 352.
 Morrow, R. (1970). Ph.D. Thesis, Flinders University.
 Morrow, R., and Brennan, M. H. (1971). *Plasma Phys.* **13**, 75.
 Pneuman, G. W. (1965). *Physics Fluids* **8**, 507.
 Stirling, A. J., and Westwood, W. D. (1968). *Rev. scient. Instrum.* **39**, 1575.
 Swanson, D. G., Gould, R. W., and Hertel, R. H. (1964). *Physics Fluids* **7**, 269.
 Woods, L. C. (1962). *J. Fluid Mech.* **13**, 570.
 Woods, L. C. (1963). *Physics Fluids* **6**, 729.